Supporting information:

LaOMS$_2$ (M = Ti, V, and Cr): Novel Crystal Spin Valves without Contact

Haoyun Bai[1], *Di Liu*[1], *and Hui Pan*[1,2]*

[1] Institute of Applied Physics and Materials Engineering, University of Macau, Macao SAR, 999078, P.R. China

[2] Department of Physics and Chemistry, Faculty of Science and Technology, University of Macau, Macao SAR, 999078, P. R. China

*Corresponding Author

H. Pan: huipan@um.edu.mo (email), +853 88224427 (tel.), +853-88222454 (fax)

Supporting notes

1. Details of Monte Carlo simulation

The Metropolis Monte Carlo (MC) simulations based on the classical Heisenberg model were carried out to estimate the Curie temperatures of LaOMS$_2$ (M = Ti, V, and Cr):

$$H = \sum_{i<j} J_{ij} \vec{S}_i \cdot \vec{S}_j + A \sum_i \vec{S}_i^{\,2}$$

where $\vec{S}_i$ is the spin operator on site *i*, $\vec{J}_{ij}$ is the exchange parameter between site *i* and *j*, and A is the single-ion magnetic anisotropy energy. The lattice parameter *a* and *b* of LaOMS$_2$ are not exactly the same, which may lead to different exchange interactions in the *x* and *y* directions. To simplify the model, the exchange interactions in the *x* and *y* directions are regarded as the same. The nearest (J$_1$), next-nearest (J$_2$) intralayer exchange, and nearest interlayer exchange (J$_3$) were considered (Figure S3). The spin exchange parameters was derived from the formula:[1]

$$E_{FM} = E_0 + 8S^2(-4J_1 - 4J_2 - 4J_3)$$

$$E_{inter-AFM} = E_0 + 8S^2(-4J_1 - 4J_2 + 4J_3)$$

$E_{A1} = E_0 + 8S^2(+4J_2)$

$E_{A4} = E_0 + 8S^2(+4J_1 + 4J_2)$

where E_0 represents the energy without the magnetic coupling. E_{FM}, $E_{inter-AFM}$, E_{A1}, and E_{A4} are the energies of the FM, inter-AFM, AFM1, and AFM4 states (Figure S3 & Table S4). Then exchange parameters was obtained as below (Table S4):

$$J_1 = \frac{E_{FM} - E_{A1}}{32S^2}$$

$$J_2 = \frac{E_{FM} + E_{inter-AFM} + 2E_{A4} - 4E_{A1}}{128S^2}$$

$$J_3 = \frac{E_{FM} - E_{inter-AFM}}{-64S^2}$$

The anisotropy energy parameter was obtained from the magnetic anisotropy energy (MAE) (Figure 2 & S9-10). The MC simulations were performed within a 16 × 16 × 1 hexagonal spin lattice containing 512 local magnetic moments. Each moment could rotate randomly and isotopically during the simulations. 40000 MC steps were performed at each temperature.

Supporting Tables

Table S1. The elastic constants (C_{11}, C_{12}, C_{22} and C_{66}) of $LaOMS_2$ (M = Ti, V, Cr, Fe, and Co).

	Ti	**V**	**Cr**	**Fe**	**Co**
C_{11}	40.610	39.250	51.647	52.508	50.319
C_{12}	5.409	4.438	17.280	14.143	2.083
C_{22}	39.587	44.800	67.994	72.168	-1.468
C_{66}	16.201	17.872	19.049	19.480	20.165
$C_{11}C_{22}-C_{12}^2$	>0	>0	>0	>0	<0

Table S2. The lattice parameter (a, b), thickness (t), the ratio of lattice constants (a/b), the total magnetic moment (Mag_{mom}), and formation energy per unitcell ($E_{f\text{-}unit}$) or ion ($E_{f\text{-}ion}$) for $LaOMS_2$ (M = Ti, V, Cr, and Fe).

	a (Å)	**b (Å)**	**t (Å)**	**a/b**	**Mag_{mom} (μ_B)**	**$E_{f\text{-}unit}$ (eV)**	**$E_{f\text{-}ion}$ (eV)**
Ti	3.88	4.032	11.154	0.962	2.000	-20.64	-2.064
V	3.893	4.068	10.472	0.957	4.000	-18.65	-1.865
Cr	3.929	4.180	9.701	0.94	6.000	-17.35	-1.735

Fe	3.835	3.932	9.793	0.975	0.052	-16.01	-1.601

Table S3. The total energies per unitcell for $LaOMS_2$ (M = Ti, V, Cr, and Fe) with (E_M) and without (E_{NM}) spin polarization, and the energy difference between them ($\Delta E = E_M - E_{NM}$)

	Ti	**V**	**Cr**	**Fe**
E_{NM} (eV)	-72.21	-71.84	-70.92	-68.63
E_M (eV)	-72.45	-72.78	-72.52	-68.63
ΔE (meV)	-241.30	-937.63	-1599.85	-0.10

Table S4. The energies of different magnetic arrangements (marked as A1-A5 and FM) for $LaOMS_2$ (M = Ti, V, and Cr) in the PBE calculations (unit: eV), the energy difference between inter-AFM and FM states per unit cell ($\Delta E = (E_{FM} - E_{inter\text{-}AFM})/4$), and the nearest neighbor exchange energy (J_1, J_2, and J_3).

	Ti	**V**	**Cr**
E_{A1}	-289.23	-290.24	-289.92
E_{A2}	-288.84	-287.25	-283.72
E_{A3}	-289.21	-289.28	-288.59
E_{A4}	-289.19	-288.30	-287.24
inter-AFM	-289.80	-291.09	-290.15
random-AFM	-289.80*	-289.10	-286.69
E_{FM}	-289.80	-291.09	-290.15
ΔE (meV)	-0.11	-0.23	-0.21
J_1 (meV)	4.295	60.577	37.169
J_2 (meV)	33.446	-16.948	-16.989
J_3 (meV)	0.028	0.014	0.006

Note: * In the optimization, the random-AFM state of $LaOTiS_2$ was finally stabilized into inter-AFM state.

Table S5. The lattice parameters (a, b) of contact structures, lattice mismatch (dif_a, dif_b), the total energy of different stacking modes (E_{s1}-E_{s3}), binding energy of the most stable stacking mode (E_b) for the $LaOCrS_2$ heterostructure. The energy of most stable stacking mode is marked in blue.

	a	**b**	**dif_a**	**dif_b**	**E_{s1}**	**E_{s2}**	**E_{s3}**	**E_b**
	(Å)	**(Å)**	**(%)**	**(%)**	**(eV)**	**(eV)**	**(eV)**	**(eV)**
Fe (100)	4.005	4.005	1.92	-4.20	-163.417	-161.335		-7.782
LFO(FeO)	3.934	3.934	0.12	-5.89	-228.086	-229.142	-228.781	-3.963
LFO(LaO)	3.934	3.934	0.12	-5.89	-228.221	-229.644	-227.417	-5.683

Table S6. The total energy (E_0), energy difference from the most stable magnetic arrangement (ΔE), and total magnetic moment of heterostructure. The energy of most stable magnetic arrangement is marked in blue.

		uuuu	**duuu**	**duud**	**uudd**	**uudu**	**dudu**
Fe/ LaOCrS_2/ Fe	**E_0 (eV)**	-167.171	-167.516	-167.860	-167.171	-167.516	-167.860
	ΔE (meV)	689.260	344.460	0.168	689.480	344.710	0.000
	mag (μ_B)	27.409	3.225	-20.904	0.000	24.118	0.000
LFO(FeO)/ LaOCrS_2/ LFO(FeO)	**E_0 (eV)**	-232.646	-232.708	-232.770	-232.647	-232.709	-232.770
	ΔE (meV)	123.890	62.320	0.560	123.340	61.650	0.000
	mag (μ_B)	17.417	5.228	-6.960	0.000	12.182	0.000
LFO(LaO)/ LaOCrS_2/ LFO(LaO)	**E_0 (eV)**	-233.177	-233.226	-233.280	-233.173	-233.226	-233.278
	ΔE (meV)	102.970	53.980	0.000	106.680	53.980	1.690
	mag (μ_B)	18.306	13.048	-7.820	0.000	13.049	0.000

Table S7. The lattice constants (a and b), magnetic moments (magmom), energies of FM and inter-AFM state (E_FM and E_inter_AFM), and energy difference between FM and inter-AFM states (ΔE = E_FM − E_inter_AFM) of LaOMS_2 under different effective U setting.

	Ti			**V**			**Cr**		
U	2	4	6	2	4	6	2	4	6
a (Å)	3.932	3.930	3.930	3.896	3.892	3.894	3.914	3.922	3.940
b (Å)	4.119	4.146	4.161	4.073	4.036	4.036	4.226	4.280	4.323
magmom (μB)	2.000	2.000	2.000	4.000	4.000	4.000	6.000	6.000	6.000
E_FM (eV)	-69.545	-67.444	-65.611	-69.519	-66.792	-64.101	-69.451	-69.394	-69.269
E_inter_AFM (eV)	-69.545	-67.444	-65.611	-69.518	-66.792	-64.100	-69.451	-69.394	-69.269
ΔE (meV)	-0.138	-0.145	-0.081	-0.316	-0.222	-0.231	-0.058	-0.021	-0.020

Supporting Figures

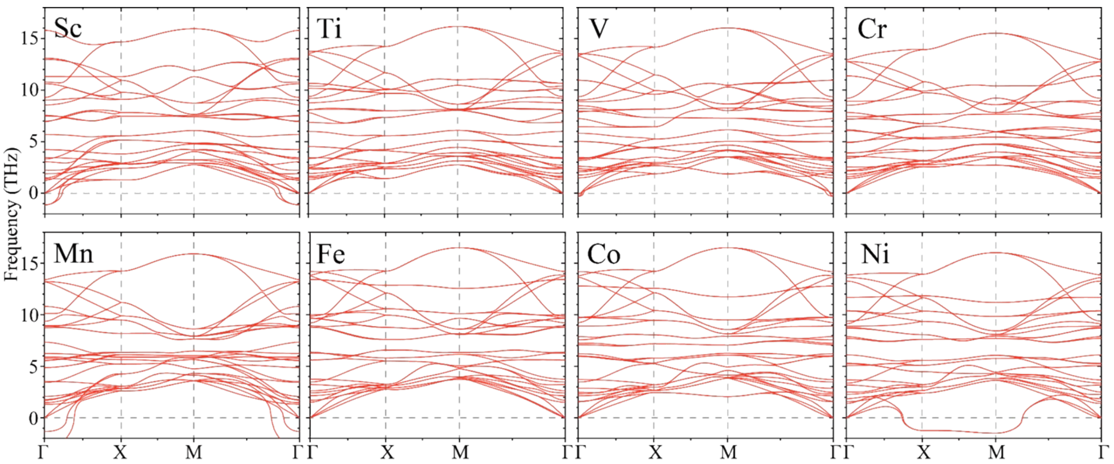

Figure S1. The phonon dispersions of $LaOMS_2$ (M = Sc, Ti, V, Cr, Mn, Fe, Co, and Ni).

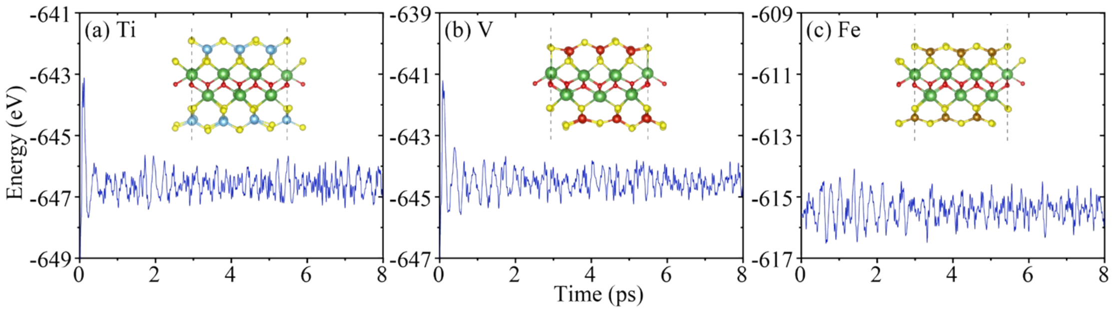

Figure S2. The AIMD simulations: (a) $LaOTiS_2$, (b) $LaOVS_2$, and (c) $LaOFeS_2$. The insets are the structure after the simulation.

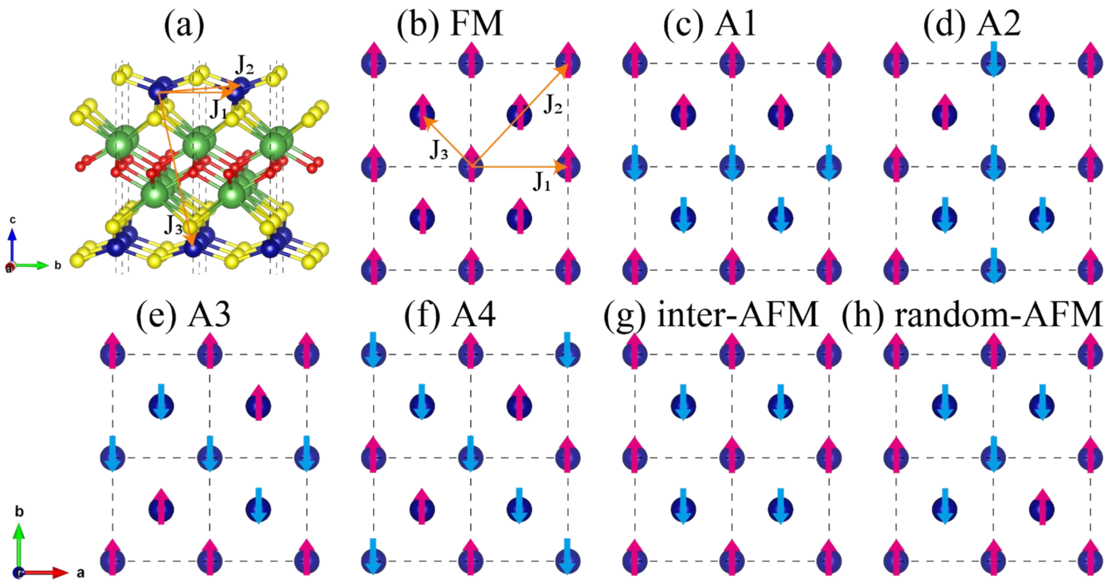

Figure S3. (a) The supercell for the magnetic arrangement of $LaOMS_2$ (M = Ti, V, and Cr). (b) ferromagnetic and (c-f) intralayer-antiferromagnetic (named A1-A4),

(g) interlayer-antiferromagnetic (inter-AFM) and (h) random antiferromagnetic configurations. The exchange interactions are denoted in orange arrows.

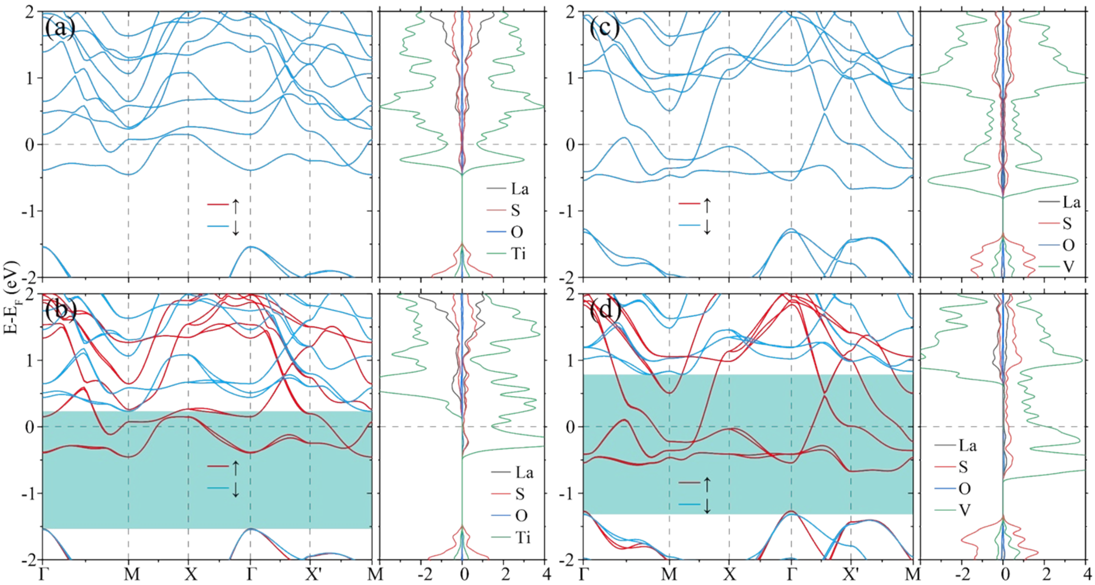

Figure S4. The band structure and DOS of $LaOTiS_2$ when in (a) inter-AFM and (b) FM state. The band structure and DOS of $LaOVS_2$ when in (c) inter-AFM and (d) FM state.

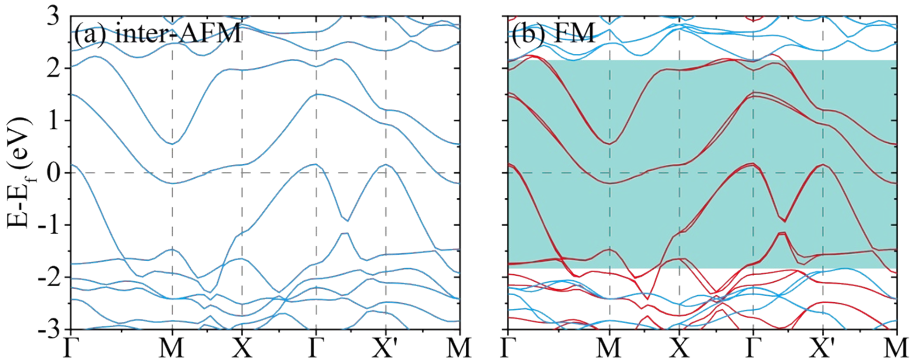

Figure S5. The band structure of $LaOCrS_2$ in (a) inter-AFM and (b) FM state calculated by the HSE06 method.

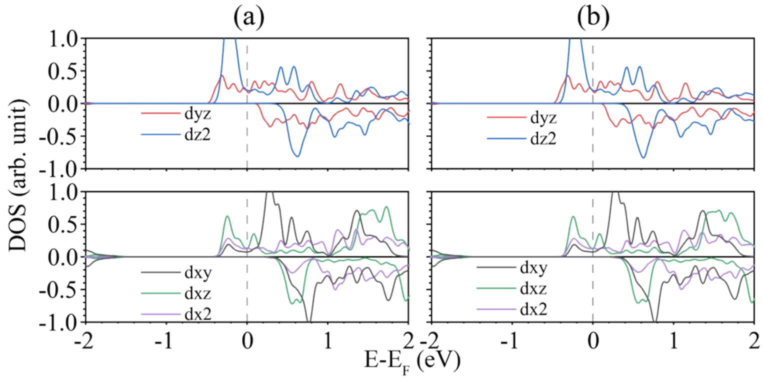

Figure S6. The PDOSs of one Ti ion in LaOTiS$_2$ in (a) inter-AFM and (b) FM state.

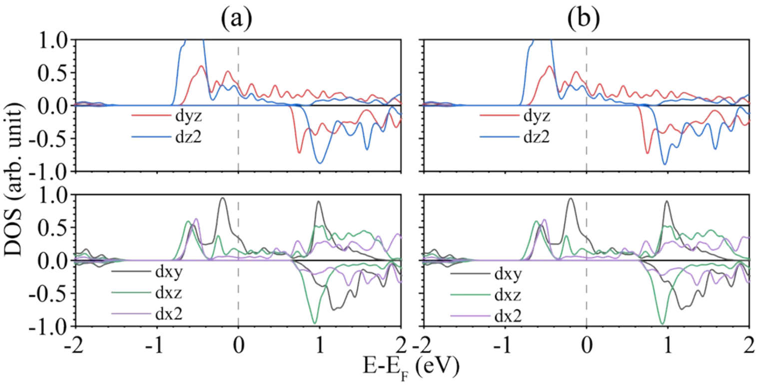

Figure S7. The PDOSs of one V ion in LaOVS$_2$ in (a) inter-AFM and (b) FM state.

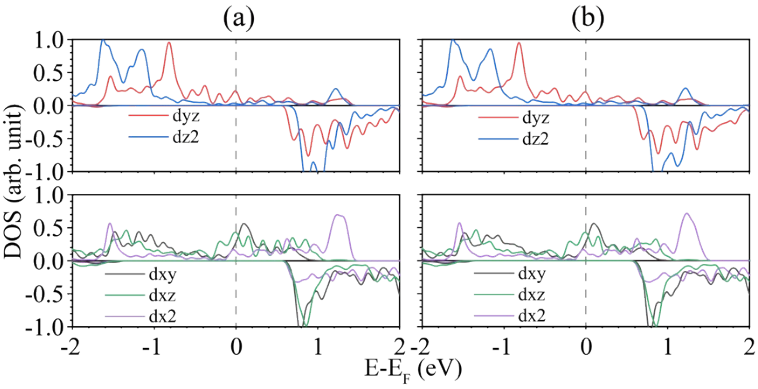

Figure S8. The PDOSs of one Cr ion in LaOCrS$_2$ in (a) inter-AFM and (b) FM state.

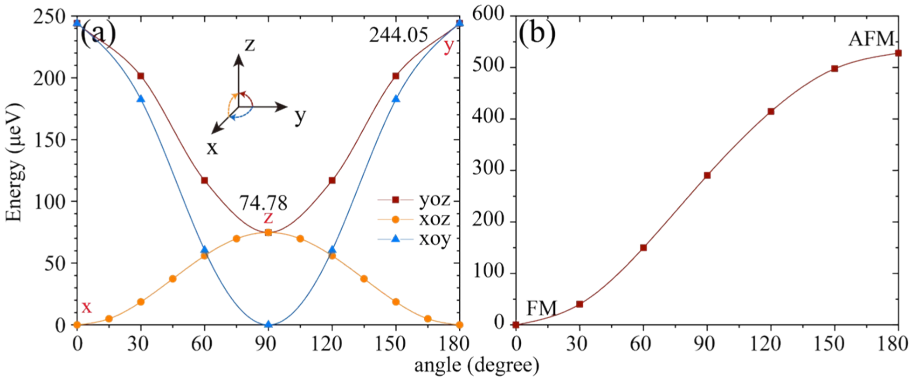

Figure S9. LaOTiS$_2$: (a) the magnetic anisotropic properties and (b) the energy profile for the switching from the AFM to FM state.

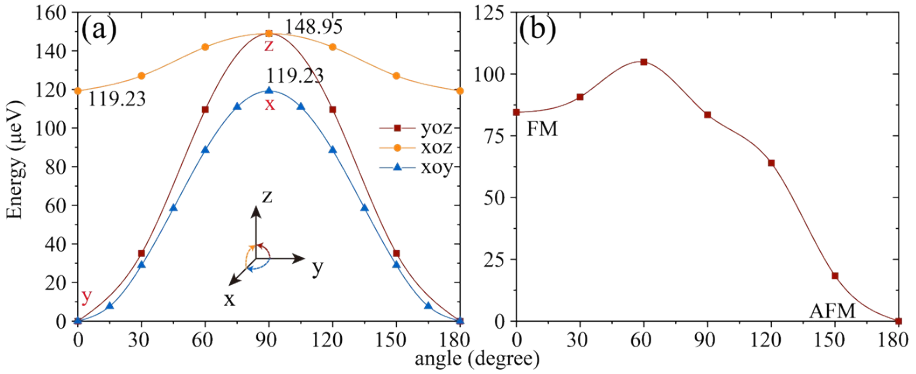

Figure S10. LaOVS$_2$: (a) the magnetic anisotropic properties and (b) the energy profile for the switching from the AFM to FM state.

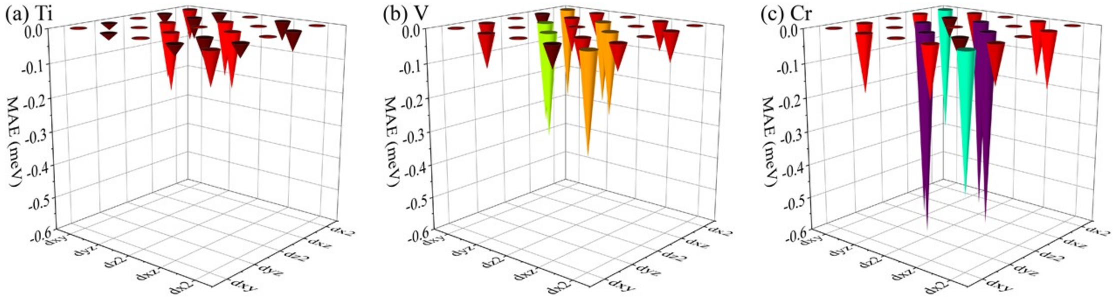

Figure S11. The d-orbital resolved MAE: (a) Ti in LaOTiS$_2$, (b) V in LaOVS$_2$ and (c) Cr in LaOCrS$_2$.

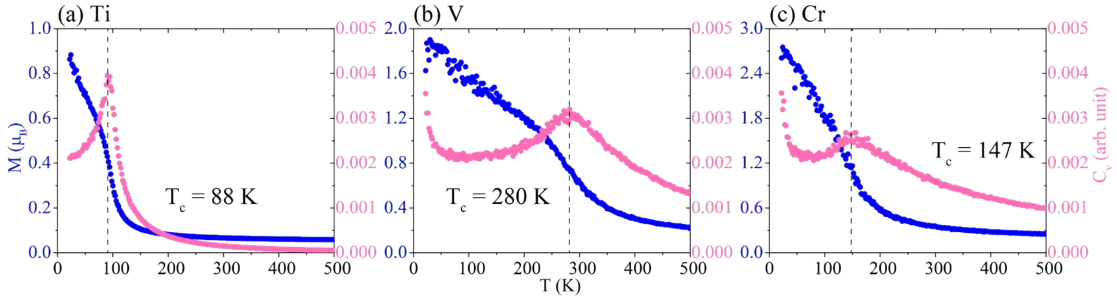

Figure S12. The simulated average magnetic moment (M) and specific heat (C_v) as the functions of temperature: (a) LaOTiS$_2$, (a) LaOVS$_2$, and (a) LaOCrS$_2$.

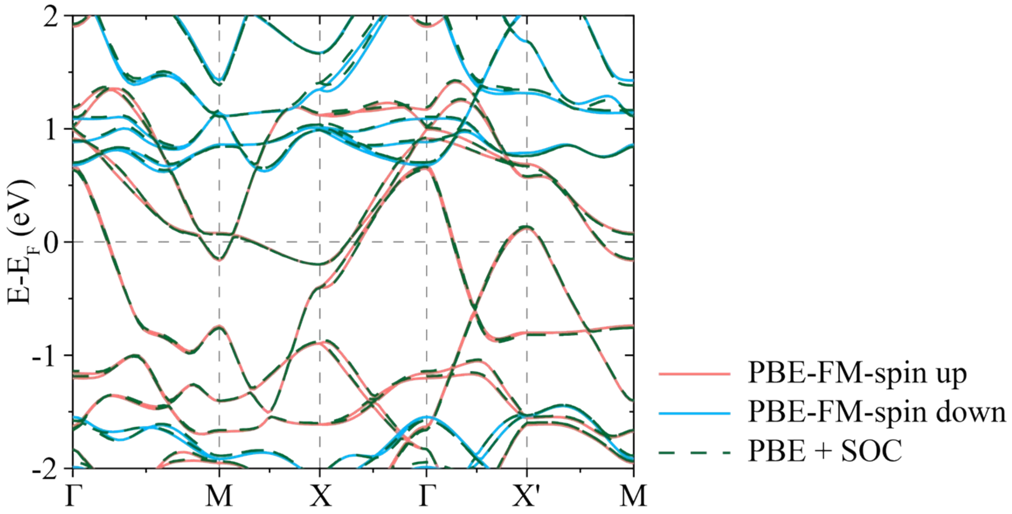

Figure S13. The PBE-FM and PBE+SOC band structures of $LaOCrS_2$.

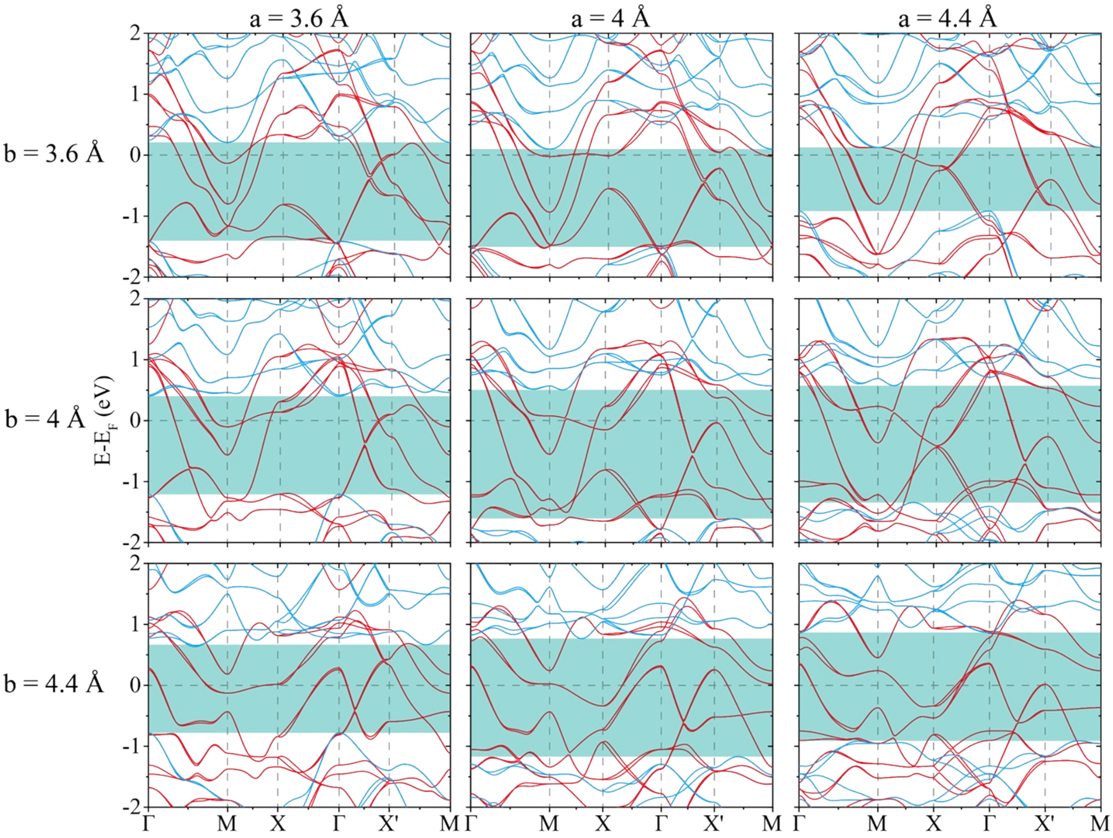

Figure S14. The band structures of FM $LaOCrS_2$ under strain. The light blue bars denote the band gaps of spin-down channels.

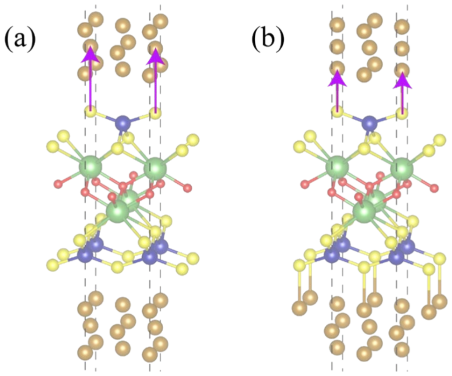

Figure S15. Possible stacking models of Fe/LaOCrS_2/Fe. (a) stack 1 and (b) stack 2. The purple arrows indicate ions with the same projected position in the *xoy* plane.

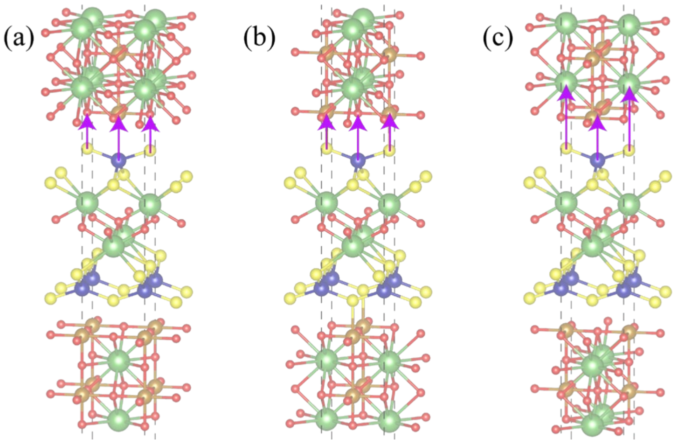

Figure S16. Possible stacking models of LFO(FeO)/LaOCrS_2/LFO(FeO). (a) stack 1, (b) stack 2 and (c) stack 3. The purple arrows indicate ions with the same projected position in the *xoy* plane.

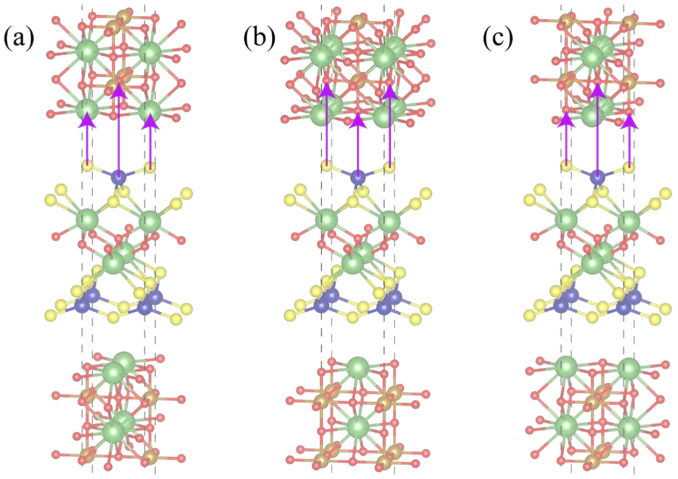

Figure S17. Possible stacking models of LFO(LaO)/LaOCrS_2/LFO(LaO). (a) stack 1, (b) stack 2 and (c) stack 3. The purple arrows indicate ions with the same projected position in the *xoy* plane.

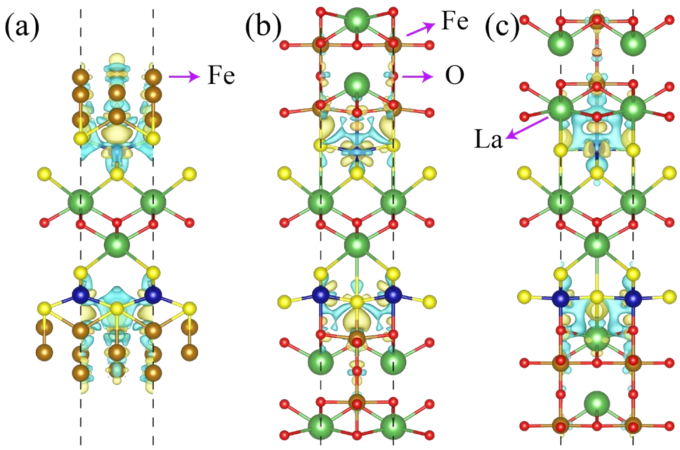

Figure S18. The optimized structure of heterostructures and charge transfer between $LaOCrS_2$ and Fe/LFO. (a) Fe/$LaOCrS_2$/Fe with stack 1, (b) LFO(FeO)/$LaOCrS_2$/LFO(FeO) with stack 2, and (c) LFO(LaO)/$LaOCrS_2$/LFO(LaO) with stack 2. The yellow and clay regions denote the charge accumulation and loss, respectively.

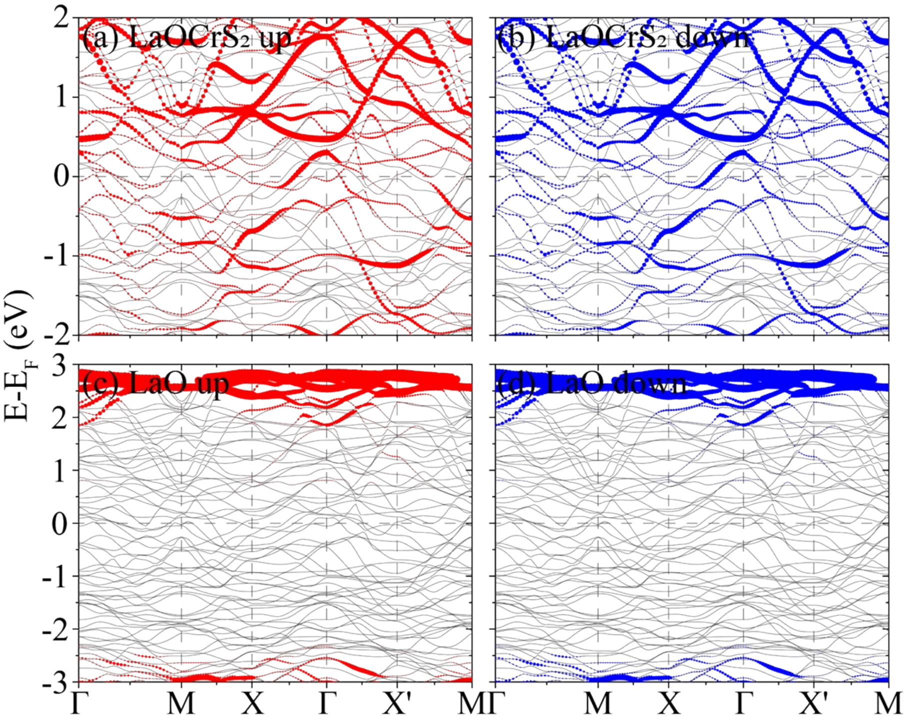

Figure S19. Fe/$LaOCrS_2$/Fe with two CrS_2 layers to be antiparallel (*dudu*) spin arrangement: the PBANDs for (a) spin-up, and (b) spin-down channel of $LaOCrS_2$, and (c) spin-up, and (d) spin-down channel of LaO.

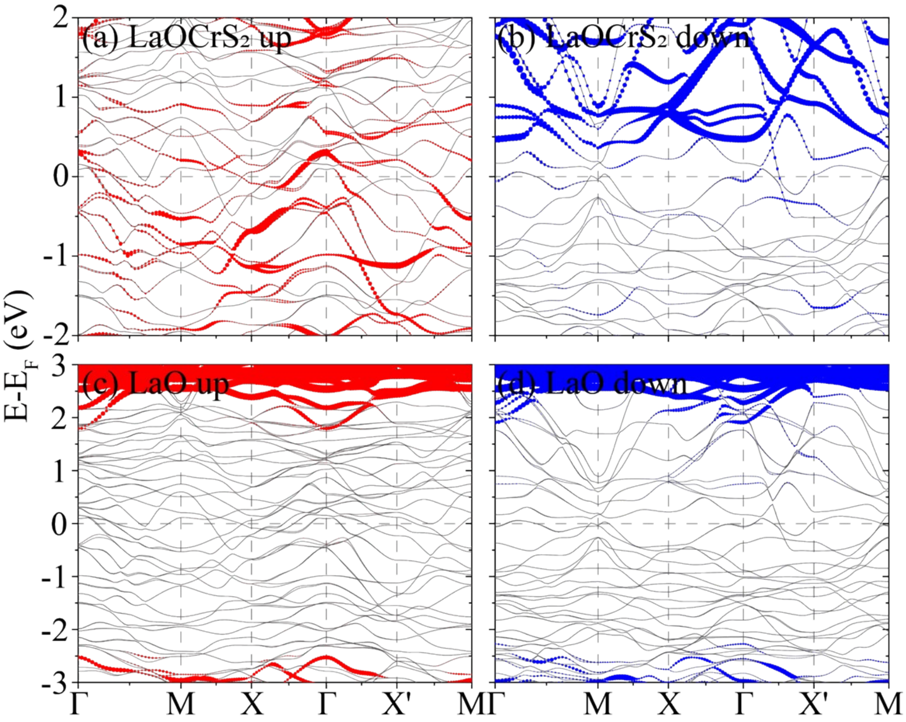

Figure S20. Fe/LaOCrS$_2$/Fe with two CrS$_2$ layers to be parallel (*duud*) spin arrangement: the PBANDs for (a) spin-up, and (b) spin-down channel of LaOCrS$_2$, and (c) spin-up, and (d) spin-down channel of LaO.

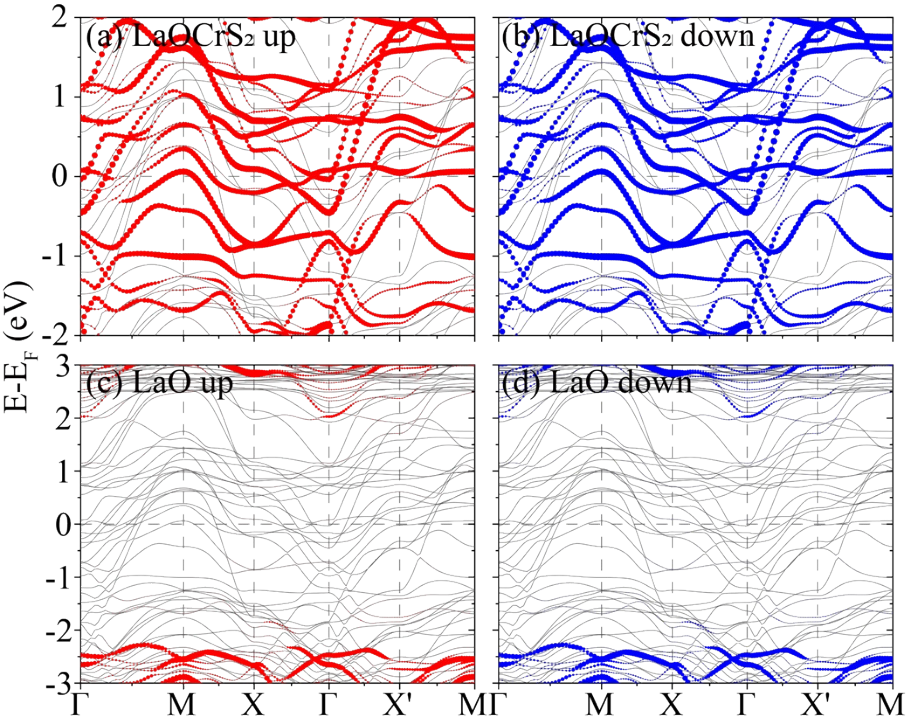

Figure S21. LFO(LaO)/LaOCrS$_2$/ LFO(LaO) with two CrS$_2$ layers to be antiparallel (*dudu*) spin arrangement: the PBANDs for (a) spin-up, and (b) spin-down channel of LaOCrS$_2$, and (c) spin-up, and (d) spin-down channel of LaO.

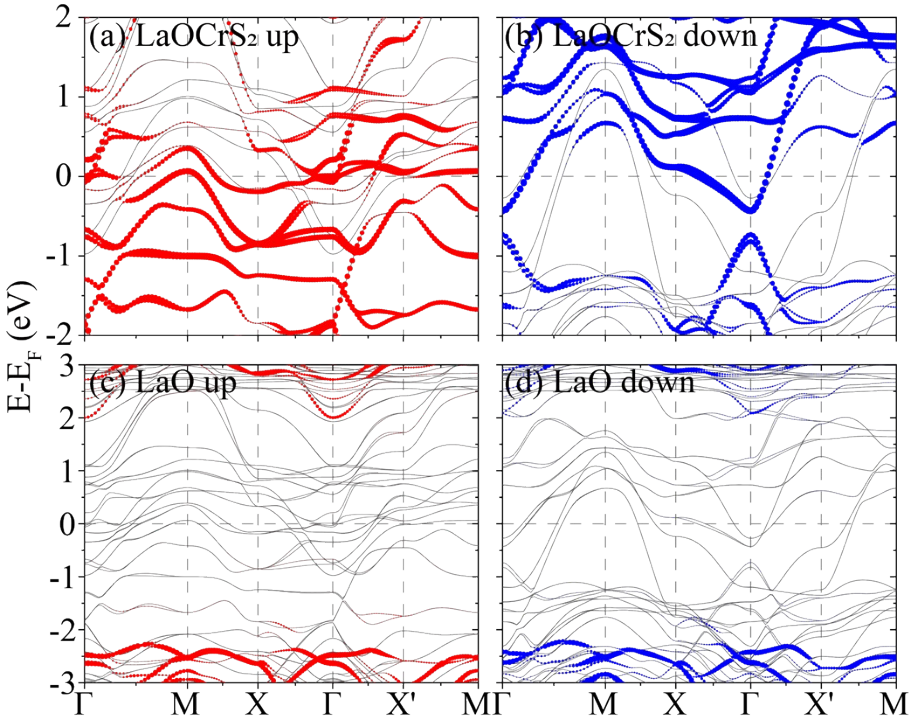

Figure S22. LFO(LaO)/LaOCrS$_2$/ LFO(LaO) with two CrS$_2$ layers to be parallel (*duud*) spin arrangement: the PBANDs for (a) spin-up, and (b) spin-down channel of LaOCrS$_2$, and (c) spin-up, and (d) spin-down channel of LaO.

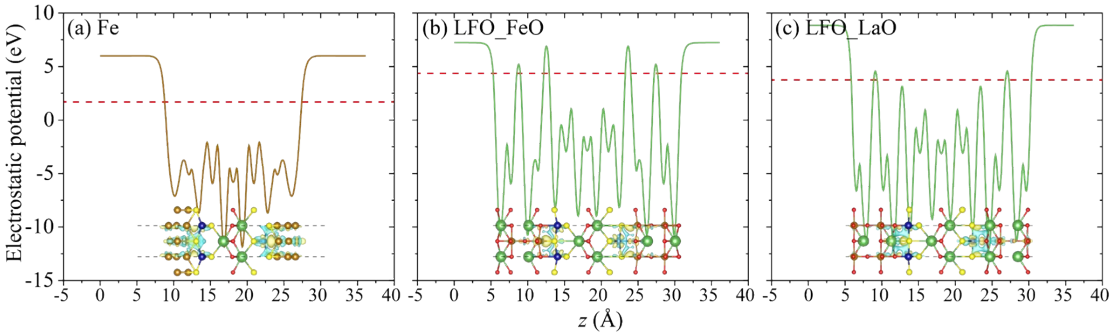

Figure S23. The electrostatic potentials: (a) Fe/LaOCrS$_2$/Fe, (b) LFO(FeO)/LaOCrS$_2$/LFO(FeO), and (c) LFO(LaO)/LaOCrS$_2$/LFO(LaO). The red dashed line is the Fermi level.

References

1. J. Deng, J. Guo and X. Chen, *Journal of the American Chemical Society*, 2020, **142**, 5234-5240.